Experimental Verification of the Stabilizing Effect of Rocket Thrust on the Dynamics of Vertical Cantilevered Columns under a Conservative Load

Bulletin of Osaka Prefecture University
Series A. Vol. 46, No. 1, 1997, pp. 61～70

Experimental Verification of the Stabilizing Effect of Rocket Thrust on the Dynamics of Vertical Cantilevered Columns under a Conservative Load

Kazuo KATAYAMA*, Yoshihiko SUGIYAMA** and Bong-Jo RYU***

(Received July 23, 1997)

The paper describes experimental observations of the effect of rocket thrust on the dynamics of cantilevered columns subjected initially to a conservative load. Four vertical test columns were set up, to which a solid rocket motor was mounted at their tip ends. Self-weight of the rocket motor made a conservative loading to the columns. The columns were then subjected to a tangential follower force which was realized as rocket thrust. FEM formulation has been made for theoretical predictions of the dynamics of the columns. The mathematical model of the columns can be characterized by a rigid body at their tip ends. Four test runs were conducted for such columns. Rocket thrust was applied to the columns which were subcritical and critical to the divergence-type instability. It was observed that the column under a conservative load oscillated with a low frequency, while under the action of rocket thrust, in addition to the conservative one, it oscillated with a higher frequency. It was even observed that a buckled column could oscillate about its vertical straight configuration when the rocket thrust was applied to the column in addition to the buckling load. Thus it was experimentally verified that a follower force induced by a solid rocket motor can stabilize dynamically a column which was subjected to a critical conservative load.

1. Introduction

The dynamic stability of elastic columns subjected to non-conservative/follower force has been the subject of a great deal of interest for structural dynamists in these decades. General aspects of the nonconservative stability problems have been compiled in the books by Bolotin[1], Leipholz[2] and Huseyin[3]. As to the origin of follower forces, rocket thrust which acts upon free-free missiles can be modeled into a tangential follower force. The dynamic stability of free-free beams subjected to a follower force has been studied by Beal[4], Matsumoto and Mote[5], and Park and Mote[6] etc..

Through the development of nonconservative stability problems, the relation between the conservative and nonconservative stability problems has been one of the interesting topics. Thus many papers[7]-[12] have been published on the stability of columns under the combined action of conservative and nonconservative forces. The conservative force can be realized easily by a dead load or a self-weight of columns. The nonconservative force can be produced as rocket thrust of a solid rocket motor which is mounted to a cantilevered column at its tip[13]-[15]. The combined action of the two kinds of forces makes a subtangential force. During the course of study of the stability problems of columns subjected to the subtangential force, it has been theoretically predicted that the subtangential force yields a higher critical force than a conservative force. However, there has been presented so far no experimental evidence for the effect of the subtangential force.

Therefore, the intended aim of this report is to describe the experimental observation of the effect of a subtangential follower force on the stability of vertical cantilevered columns. Self-weight of a solid rocket motor fixed at the free end of the column makes a conservative loading which acts on the column initially, while rocket thrust of the motor yields a nonconservative loading which acts on the column in addition to the conservative one, thus the total compressive load is much more greater than the buckling load of the considered column. The present report will give an experimental observation that application of rocket thrust to a column under the action of critical conservative force can make the column dynamically stable as long as the thrust acts on the column.

2. Mathematical Model

Figure 1 shows a mathematical model of a vertical cantilevered column subjected to a subtangential force. The column is assumed to be a slender uniform column. The force can be produced by the combined action of rocket thrust and self-weight of the rocket motor. In Fig. 1, ρ is the density of the uniform column, A the cross-sectional area of the column, M the

*Part-time Doctoral Student, Department of Aerospace Engineering, College of Engineering; Manager, Daicel Chemical Industries, Ltd.
**Department of Aerospace Engineering, College of Engineering.
***Department of Mechanical Design Engineering, Taejon National University of Technology, Taejon, Korea.

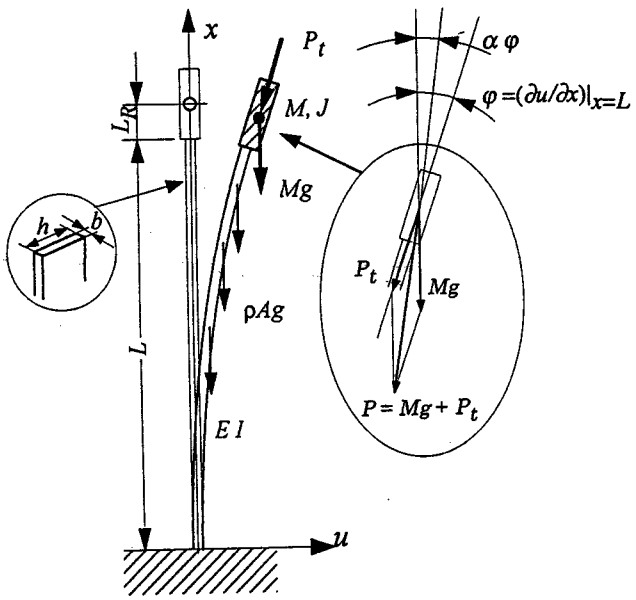

Fig.1 Mathematical model of a vertical cantilevered column

mass of the rocket motor, J the rotary inertia of the rocket motor, and L_R means the distance between the free end of the column and the mass center of the rocket motor. The rocket motor is considered as a rigid body, not a mass point as it has been assumed in many papers published so far[1]. The subtangential force can be represented as the resultant vector P of a vertical force Mg and a pure tangential follower thrust P_t. The direction of the resultant subtangential force is specified by $\alpha\varphi$ as shown in Fig. 1, where φ is the angle of inclination of the tangent at the tip end. The parameter α can specify the angle between the direction of the resultant force and the z-axis and it is called "tangency coefficient". When α=0, the direction of the force is vertical, i.e. the force is conservative. When α =1.0, it is tangential to the tip end, i.e. the force is purely nonconservative. Thus the coefficient α is sometimes referred to as the nonconservativeness parameter.

3. Finite Element Formulation

The energy expressions for the above mathematical model can be written in the forms;

$$T=\frac{1}{2}\int_o^L \rho A\left(\frac{\partial u}{\partial t}\right)^2 dz+\frac{1}{2}M\left[\frac{\partial u}{\partial t}+L_R\frac{\partial^2 u}{\partial t\partial z}\right]_{z=L}^2+\frac{1}{2}J\left[\left(\frac{\partial^2 u}{\partial t\partial z}\right)^2\right]_{z=L} \quad (1)$$

$$V=\frac{1}{2}\int_o^L EI_y\left(\frac{\partial^2 u}{\partial z^2}\right)^2 dz, \quad (2)$$

$$Wc=\frac{1}{2}\int_o^L (P_t+Mg)\left(\frac{\partial u}{\partial z}\right)^2 dz, \quad (3)$$

$$\delta Wnc=-P_t\left[\frac{\partial u}{\partial z}\delta u\right]_{z=L}, \quad (4)$$

$$Wsw=\frac{1}{2}\int_o^L \rho Ag(L-z)\left(\frac{\partial u}{\partial z}\right)^2 dz. \quad (5)$$

In the above expressions, T is the total kinetic energy of the considered system, V the potential energy, W_c the work done by the conservative component of the subtangential force, δW_{nc} the virtual work done by the nonconservative component of the subtangential force, W_{sw} the work done by self-weight of the column.

In order to derive the equation of motion, let us start with the following extended Hamilton's principle;

$$\delta\int_{t_1}^{t_2}(T-V+W_c+W_{sw})dt+\int_{t_1}^{t_2}\delta W_{nc}dt=0. \quad (6)$$

Substitution of Eqs.(1)-(5) into Eq.(6) leads to

$$\int_{t_1}^{t_2}\left\{\int_o^L\left[EI_y\frac{\partial^2 u}{\partial z^2}\delta\left(\frac{\partial^2 u}{\partial z^2}\right)+\rho A\frac{\partial^2 u}{\partial t^2}\delta u-P\frac{\partial u}{\partial z}\delta\left(\frac{\partial u}{\partial z}\right)-\rho Ag(L-z)\delta\left(\frac{\partial u}{\partial z}\right)\right]dz\right.$$
$$+M\left[\frac{\partial^2 u}{\partial t^2}\delta u\right]_{z=L}+ML_R\left[\frac{\partial^2 u}{\partial t^2}\delta\left(\frac{\partial u}{\partial z}\right)+\frac{\partial^3 u}{\partial t^2\partial z}\delta u\right]_{z=L}$$
$$\left.+(ML_R^2+J)\left[\frac{\partial^3 u}{\partial t^2\partial z}\delta\left(\frac{\partial u}{\partial z}\right)\right]_{z=L}+\alpha P\left[\frac{\partial u}{\partial z}\delta u\right]_{z=L}\right\}dt=0, \quad (7)$$

where $P = Mg + P_t$ and $\alpha = P_t/P$.

In order to obtain a characteristic equation related to the flexural vibration of the column, let us rely on finite element formulation. Now, the column is divided into N segments having an equal length l, as shown in Fig. 2.

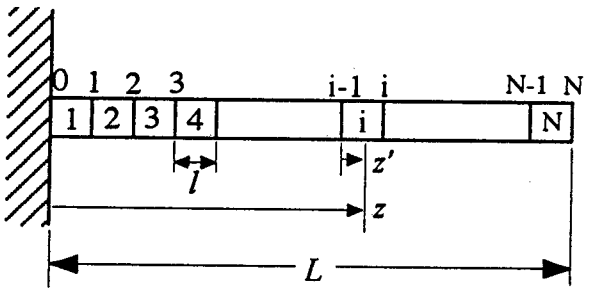

Fig.2 Finite elements

For convenience of dealing with the equations in dimensionless forms, the following dimensionless quantities are introduced;

$$z'=z-(i-1)l,\quad \xi=z'/l,\quad \eta=u/l, \quad (8)$$

where i (=1,2,3,$\cdots$,N) is an integer.

Now the dimensionless displacement η can be assumed to take the form

$$\eta(\xi,t)=\eta(\xi)e^{st}. \tag{9}$$

Substitution of Eq.(9) into Eq.(7), together with the expressions(8), results in the following matrix form;

$$\sum_{i=1}^{N}\left\{\frac{\lambda^2}{N^4}\delta H_i^T[m]H_i+\delta H_i^T[k]H_i-\frac{T}{N^2}\delta H_i^T[p]H_i-\delta H_i^T[w]H_i\right\}$$

$$+\frac{\lambda^2\bar{M}}{N^3}\delta H_N^T\bar{M}_F H_N+\frac{\lambda^2\bar{M}\bar{L}_R}{N^2}(\delta H_N^T\bar{L}_{1F}H_N+\delta H_N^T\bar{P}_{tF}H_N)$$

$$+\lambda^2\left(\frac{\bar{M}\bar{L}_R^2}{N^2}+\frac{\bar{J}}{N}\right)\delta H_N^T\bar{J}_F H_N+\alpha\frac{T}{N^2}\delta H_N^T\bar{P}_{tF}H_N=0, \tag{10}$$

where the dimensionless parameters are defined as follows;

$$\lambda^2=\frac{\rho AL^4\varsigma^2}{EI_y},\ T=\frac{PL^2}{EI_y},\ \bar{M}=\frac{M}{\rho AL},\ \bar{J}=\frac{J}{\rho AL^3},$$

$$\bar{L}_R=\frac{L_R}{L},\ \alpha=\frac{P_t}{Mg+P_t}=\frac{P_t}{P}. \tag{11}$$

In Eq.(10), the following shape function vector $a(\xi)$ satisfying the compatibility condition, and the nodal displacement vector Hi are introduced:

$$a^T(\xi)=\{1-3\xi^2+2\xi^3,\ \xi-2\xi^2+\xi^3,\ 3\xi^2-2\xi^3,\ -\xi^2+\xi^3\}, \tag{12}$$

$$H_i^T=\{\eta_{i-1},\ \eta'_{i-1},\ \eta_i,\ \eta'_i\}. \tag{13}$$

Finally, Eq.(10) can be written in the global characteristic equation

$$\{[K^*]+\lambda^2[M^*]\}\{G\}=0, \tag{14}$$

where {G} means the generalized coordinate vector, and $[K^*]$ and $[M^*]$ denote the global stiffness matrix and the global mass matrix, respectively.

The stability of the system under consideration is determined by the sign of eigenvalue λ^2. The stability criterion are as follows;

$$\mathrm{Re}(-\lambda^2)>0,\quad \mathrm{Im}(-\lambda^2)=0 \quad ;\text{stable} \tag{15}$$

$$\mathrm{Re}(-\lambda^2)<0,\quad \mathrm{Im}(-\lambda^2)=0 \quad ;\text{divergence} \tag{16}$$

$$\mathrm{Re}(-\lambda^2)>0,\quad \mathrm{Im}(-\lambda^2)\neq 0 \quad ;\text{flutter} \tag{17}$$

4. Rocket Motor and Test Beams

The rocket motors used in the present experiment are small-sized solid rocket motors designed for the combustion test of propellant. The motors were made by Daicel Chemical Industries, Ltd.. A detail plan of the rocket motor is shown in Fig. 3. The thrust curve of the rocket motor is shown in Fig. 4. Initial mass of the rocket motor including propellant of 0.9kg is given in Table 1. The nominal initial mass of the motor is assumed to be 14.65kg. The rotary inertia J of the rocket motor and the distance L_R between the center of gravity of the rocket motor and the free end of the column were J=0.1196 kg·m² and L_R=200mm, respectively. Test beams in the present experiment have the width b=30mm, and the thickness h=8mm, 9mm. The beams were made of aluminum. The density ρ =2672 kg/m³, and Young's modulus E=6.903×10³ kg/mm², which was found by the bending test described later.

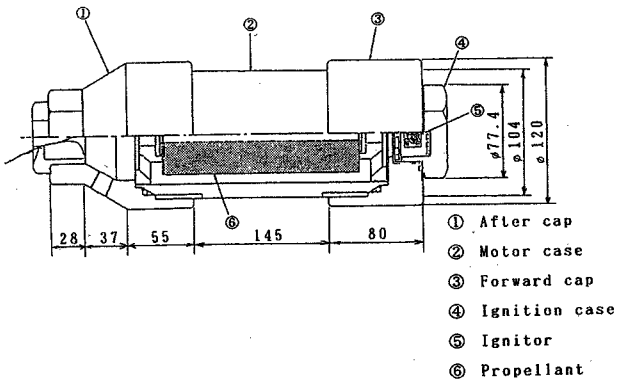

Fig. 3 Plan of solid rocket motor

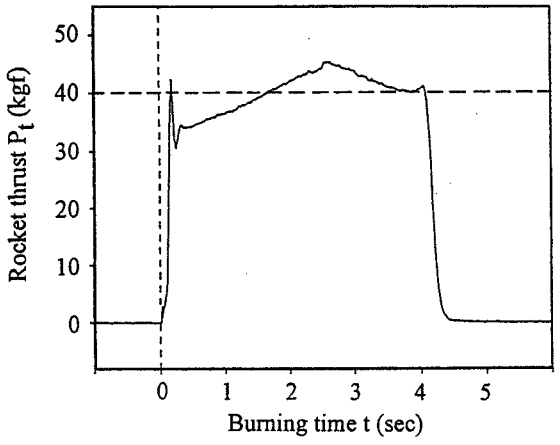

Fig. 4 Thrust curve

Table 1. Mass of the rocket motor.

Number of rocket motor	Mass (kg)
Rocket motor No.1	14.65
Rocket motor No.2	14.60
Rocket motor No.3	14.70
Rocket motor No.4	14.60

5. Static Bending Test

5.1 Bending stiffness of beams

In order to correctly predict instability boundaries by calculation, it is needed to know the exact bending stiffness of

test beams. The bending stiffness EI can be obtained by the bending test of the beam, as shown in Fig. 5. When a concentrated lateral force W is acted upon the beam at the position a apart from the free end of the beam, the displacement d at the point c apart from the free end is given by

$$d = \frac{(L-a)^2(2L+a-3c)W}{6EI} \tag{18}$$

This is a well known formula in a textbook of the strength of materials. Therefore, the bending stiffness of the beam EI can be obtained by the following expression;

$$EI = \frac{(L-a)^2(2L+a-3c)W}{6} \cdot \frac{W}{d} \tag{19}$$

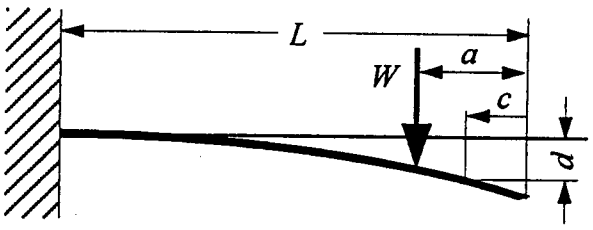

Fig. 5 Horizontal cantilevered beam

5.2 Static bending test of beams

Figure 6 depicts the sketch of the static bending test of a beam. The procedure of the static test can be read as follows;

① Two test beams were provided, and then the dimensions of the test beams were measured. The measured dimensions of the test beams were as follows;

Test beam(A); width b=30mm, thickness h=8mm, length L=1331mm

Test beam(B); width b=30mm, thickness h=9mm, length L=1481mm

The acting position a of the lateral force and the measuring point c were assumed to have the same values for the two test beams and they were taken to be a=70mm and c=10mm.

② Horizontal of the test beams was checked by a water level.

③ In order to apply the concentrated lateral force W at the position a, a small dish was hung from the test beam c apart from the tip end, and then put a counter-weight on the dish.

④ Displacement d was read by a microscope. The displacement d was kept within 1% of the length of the test beam.

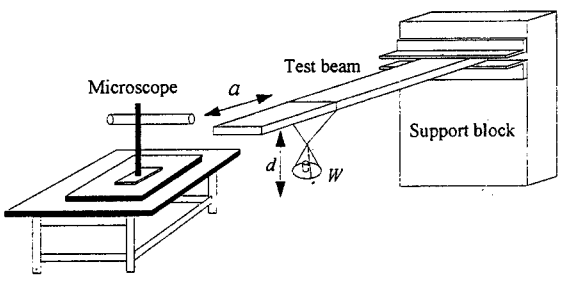

Fig. 6 Sketch of static bending test

5.3 Calculation of Young's modulus

Figure 7 shows the relation between the applied force W and the displacement d for the two test beams. The value of d/W was obtained from Fig. 7;

Test beam(A) : d/W = 0.0249 (m/kgf)

Test beam(B) : d/W = 0.0295 (m/kgf)

Therefore, the experimental bending stiffness EI given by Eq.(19) yielded experimental Young's modulus of test beams;

$E = 6.903 \times 10^3$ (kg/mm^2)

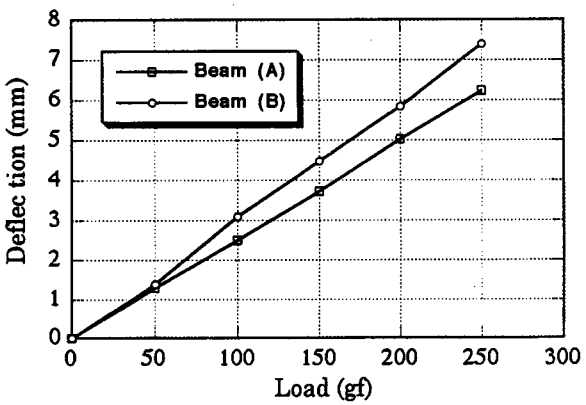

Fig. 7 Load-displacement relation

6. Numerical Results

6.1 Eigenfrequency of test columns

As to the basic dynamics of the columns in the present experiment, the first and second eigenfrequencies of the columns with and without the rocket thrust were calculated by the characteristic equation(14). The frequencies of the columns with and without the thrust for the test column No. 2(see Table 2) are plotted in Figs. 8(a) and 8(b). In Fig. 8(a), the points C_1 and C_2 denote the first and second eigenfrequency of the column under the conservative loading due to the rocket motor, respectively. The point D_1 and D_2 mean the first and second divergence force, respectively, while the point F represents the flutter point on the eigenvalue curve for α=0.74. In Fig. 8(b), the curve AC_1 shows the first eigenfrequency for a conservative loading(α=0), while the curve BC_1 depicts the frequency for a subtangential loading of α=0.74(refer to Eq.(20) given later).

6.2 Stability maps of the test columns

Type of instability of the columns depends on the tangency

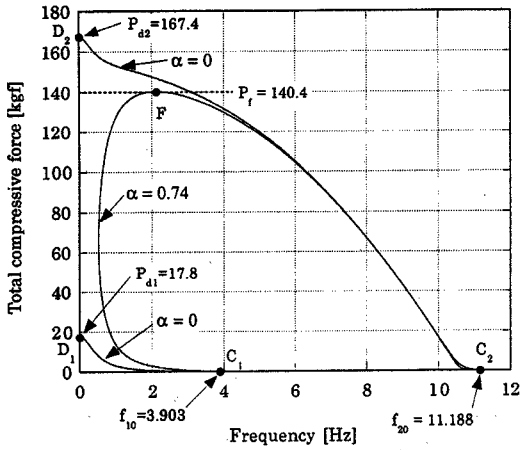

(a) First and second eigen frequencies

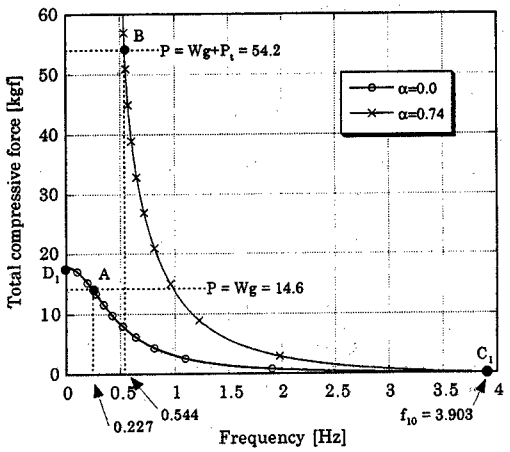

(b) Details of the first eigenfrequency curves

Fig. 8 Compressive load-frequency relation for test run No. 2

coefficient α of the total compressive force($Mg+P_t$). When the tangency coefficient of the rocket thrust is changed from zero to unity, the divergence-type instability in the first mode can take place for the coefficient $\alpha \leqq 0.5$, while for $\alpha > 0.5$ flutter-type instability can occur. Typical stability maps of the test columns are shown in Fig. 9. These maps also contain the broken curves which show the relation between the total compressive force $P=Mg+P_t$ and tangency coefficient α. The curves are plotted on the assumption that the conservative load Mg is fixed to be 14.2kgf, while the rocket thrust P_t is increasing from zero.

In the actual experiment, the rocket thrust P_t is assumed constant and 40kgf. Thus the tangency coefficient α is taken as

$$\alpha = 40/(14.2+40) = 0.74, \tag{20}$$

where the average weight of the rocket motor during burning is taken as 14.2 kgf, since it was assumed that the initial weight of the motor is 14.65 kgf and the weight of the propellant is 0.9 kgf (thus the final weight of the motor is 14.65-0.9=13.75 kgf).

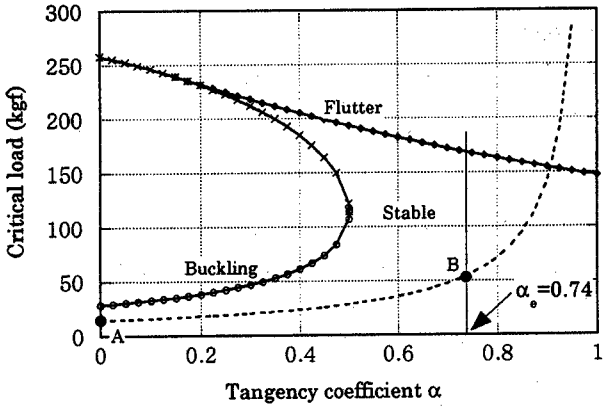

(a) Test column No. 1

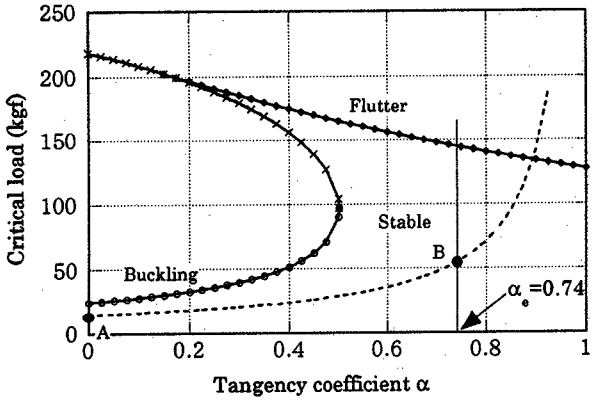

(b) Test column No. 2

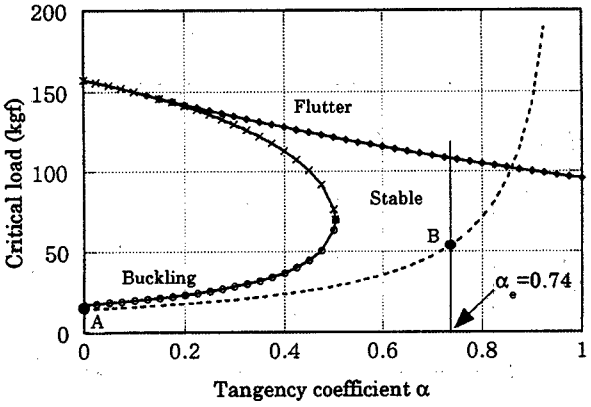

(c) Test column No. 3

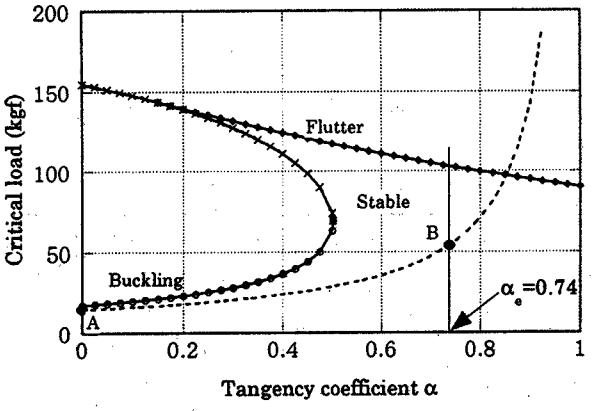

(d) Test column No. 4

Fig. 9 Stability maps in load-tangency coefficient plane

6.3 Design of the test columns

Since one run of a rocket motor is expensive, only four test runs were planned in the present experimental project. Thus detailed considerations on the design of the test columns were needed. The stability limits of the total compressive force acted upon the columns having different dimensions are shown in Table 2. Relation between buckling load and length of columns are shown in Figs. 10(a) and 10(b) for different thickness of the columns. Table 3 depicts the buckling length of the four test columns. It is noted that the applied conservative force was fixed as 14.65 kgf.

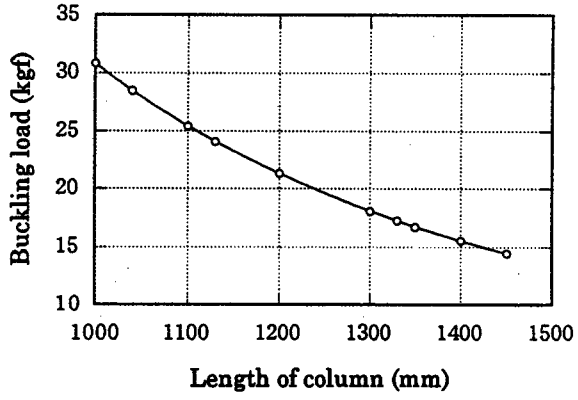

(a) Column with thickness of 9 mm

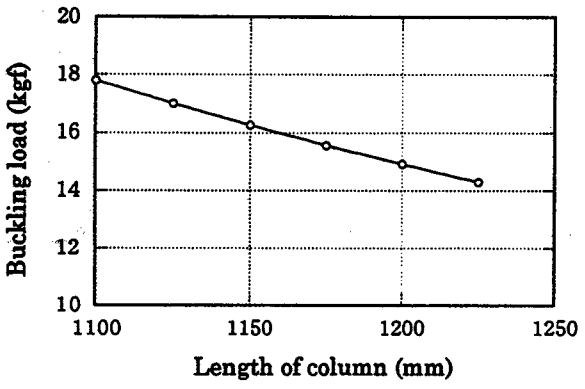

(b) Column with thickness of 8 mm

Fig. 10 Buckling load-column length relation

Table 2. Details of the candidate columns.

Width (mm)	Thickness (mm)	Length (mm)	Buckling load (kgf)	Flutter load (kgf)	Transition of state	Column No.
30	9	1000	30.83	180.97	S=>S*	
30	9	1040	28.48	168.64	S=>S	No. 1
30	9	1100	25.42	152.40	S=>S	
30	9	1130	14.07	145.16	S=>S	No. 2
30	9	1200	21.30	130.15	S=>S	
30	9	1300	18.09	112.45	S=>S	
30	9	1330	17.26	107.84	S=>S	No. 3
30	9	1350	16.74	104.93	S=>S	
30	9	1400	15.54	98.13	S=>S	
30	9	1450	14.45	91.97	D=>S**	
30	8	1100	17.81	107.17	S=>S	
30	8	1125	17.01	102.91	S=>S	No. 4
30	8	1150	16.27	98.89	S=>S	
30	8	1175	15.57	95.10	S=>S	
30	8	1200	14.91	91.53	S=>S	
30	8	1225	14.29	88.16	D=>S	

*: 'S=>S' denotes the transition from a stable state with a low frequency to another stable state with a higher frequency.

**: 'D=>S' denotes the transition from a buckled state to a dynamically stable state.

Table 3. Buckling length of the column

Column	Conservative load *Mg*	Thickness	Buckling length
No. 1	14.65 kgf	9 mm	1435 mm
No. 2	14.60 kgf	9 mm	1440 mm
No. 3	14.70 kgf	9 mm	1430 mm
No. 4	14.60 kgf	8 mm	1210 mm

(The width of the columns is fixed to be 30mm)

7. Test Runs with Rocket Thrust

7.1 Outline of experiment

The intended aim of the present experiment is to demonstrate the stabilizing effect of rocket thrust on the dynamics of cantilevered columns, which are initially subjected to a conservative load. As seen in Fig. 8(b), the first eigenfrequency decreases as the conservative load (α=0) increases, while it decreases slowly as the subtangential load of α=0.74 increases. It is now confirmed that the term "stabilizing" effect here implies "higher" frequency. Four stability maps in Fig. 9 depict straightforward the state of stability of the column when it was subjected to a conservative load of α=0 and to a subtangential load of α=0.74. In Figs. 8(b) and 9(a), (b), (c), (d), the point A means the column under a conservative load (α=0), while the point B the column under a subtangential load of α=0.74. When the tangency coefficient α=0, the column loses its stability by divergence i.e., buckling. When the coefficient α=0.74, the column loses its stability by flutter. It is noted that the flutter load is much more higher than the divergence one, as seen by Fig. 8(a). Application of rocket thrust to the column in addition to a conservative load can change the type of instability. This is the physical mechanism of the stabilizing effect of rocket thrust.

Through detailed consideration of Table 3 and Fig. 9, the present experiment are focused on demonstrating the following two cases;

Case 1 : Initially the column under a conservative load sways with a low frequency, since the load is close to but lower than the buckling load. Then the rocket thrust of 40 kgf will be applied to the column. The column may oscillate with a higher frequency during the burning of the rocket motor. After the burn out of the motor, the column shall again sway with a low frequency.

Case 2 : Initially the column under the buckling load is at rest in a bent configuration. Then the rocket thrust of 40 kgf is applied to the column in addition to the conservative buckling load. The application of the rocket thrust may make the column dynamically stable as long as the thrust is alive. After the burn out, the column shall again have the bent configuration.

Figure 11 shows the sketch of the experimental setup. A vertical column was cantilevered upward and equipped with a solid rocket motor at its free end. The free end was loosely harnessed by two thin wires which prohibited the column to sway out extremely, but allow it to oscillate freely with small and moderate amplitude. Figure 12 shows the photographs of the experimental setup. Measuring devices were installed for axial compressive strain and lateral displacement of the test columns. Dynamic behavior of the columns was recorded by a video camera and a motor-driven camera.

It is again noted that the nominal weight of the motor before ignition was 14.65 kgf, while the weight of the propellant was

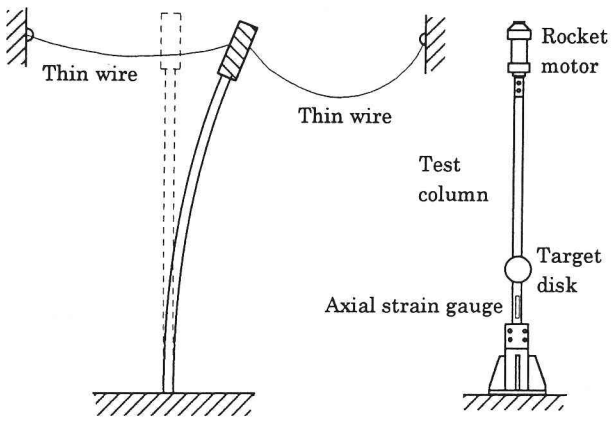

Fig. 11 Conceptual sketch of experimental setup

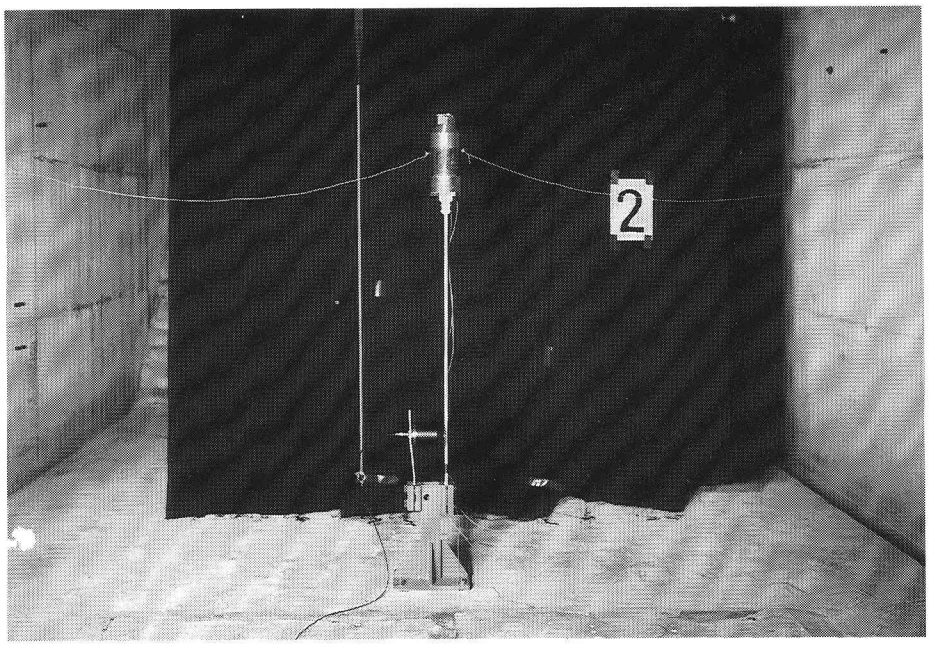

(a) Total view of the setup

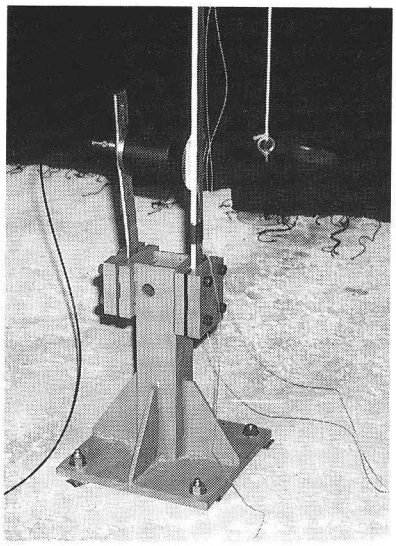

(b) Bottom end of the vertical column

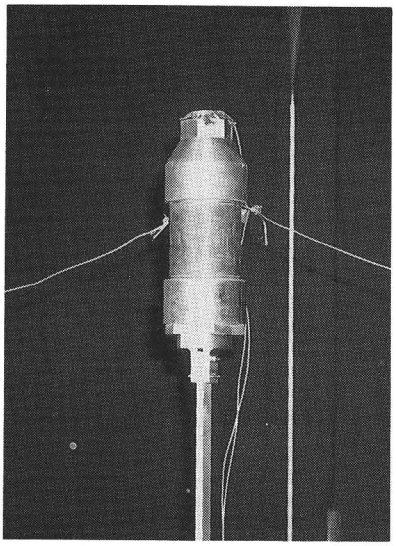

(c) Rocket motor mounted at the tip end of the column

Fig. 12 Photographs of experimental setup

0.9 kgf. This means that the weight of the motor after burn out was 13.75 kgf. Thus the average weight of the motor during burning was 14.2 kgf. The rocket thrust was assumed to be constant and of 40 kgf during the burning period of 4 seconds.

7.2 Results of experiments

Four test runs were conducted in the present experiments.

Test run No. 1: This test run corresponds to the stability map shown in Fig. 9(a). The dimensions of the test column were given in Table 2; the length of the column is 1040mm, the width 30mm and the thickness 9mm. The vertical column without rocket thrust swung with a low frequency and rather a large amplitude. Under the action of rocket thrust, it oscillated with a higher frequency and a smaller amplitude. After burn out of the rocket, it again swung as it was before ignition.

Test run No. 2: The run corresponds to the stability map shown in Fig. 9(b). The dimension of the column were given in Table 2; the length of the column is 1130mm, the width 30mm and the thickness 9mm. Since the test column of the run No. 2 had a longer length than that of No. 1, the former oscillated with a lower frequency than the latter. Recorded displacement and axial strain were shown in Fig. 13. It was observed that the column under a conservative load oscillated with a low frequency, and that, under a rocket thrust in addition to the conservative load, it oscillated with a higher frequency. Table 4 shows the comparison of the first eigenfrequency obtained by theory(refer to Fig. 8(b)) and experiment(see Fig. 13) for test run No. 2.

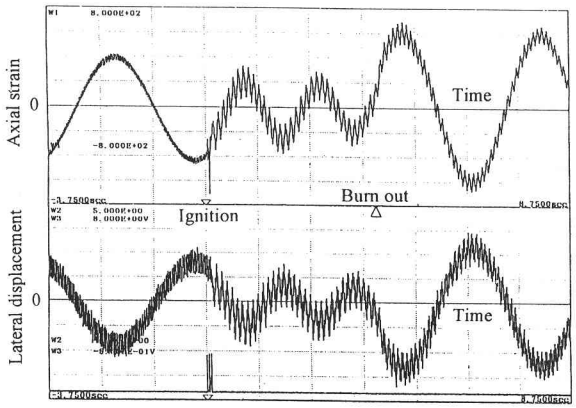

Fig. 13 Recorded axial strain and displacement for test run No. 2

Table 4. First eigenfrequency of the column in test run No.2.

	Without rocket thrust α=0	With rocket thrust α=0.74
Theory	0.227 Hz	0.544 Hz
Experiment	0.29 Hz	0.66 Hz

Test run No. 3: The stability map shown in Fig. 9(c) predicts the stability behavior in this test run. The dimensions of the test column were given in Table 2 and they were 1330 x 30 x 9 mm. The length of the test column was chosen to close to the critical length for buckling. Because of the offset between the free end of the column and the center of weight of the motor (therefore the offset caused a bending moment to the column at its free end), the column could bent even when the weight of the motor is slightly lower than the buckling load. Thus the column without rocket thrust was in the state of bent

configuration. Application of rocket thrust yielded the total compressive load of 14.65 + 40 kgf. At the moment of the application of rocket thrust, the bent column stood up and began to swing with a moderate frequency. After the burn out of the motor, the column swung with a very low frequency. The reason why the column could not retain its bent configuration was that all the propellant was consumed and thus the weight of the motor after the burn out was deceased by 0.9 kgf.

Test run No. 4: The stability map shown in Fig. 9(d) depicts the stability behavior in this run. The dimensions of the column were given in Table 2 and they were 1125 x 30 x 8 mm. The dimensions were chosen to realize the critical state for buckling. Because of the effect of offset of the conservative load(the weight of the motor), the column was in the state of bent configuration. Under the combined action of the motor's weight and rocket thrust, the column oscillated with a moderate frequency around the undeformed configuration. After the burn out of the motor, the column retained its bent configuration.

A sequence of frames of the column's behavior observed in the test run No. 4 was shown in Fig. 14. Figure 15 depicts the records of the axial strain and dynamic displacement in the test run No. 4. The records demonstrates the stabilizing effect of rocket thrust on the dynamics of the column subjected initially to the conservative buckling load.

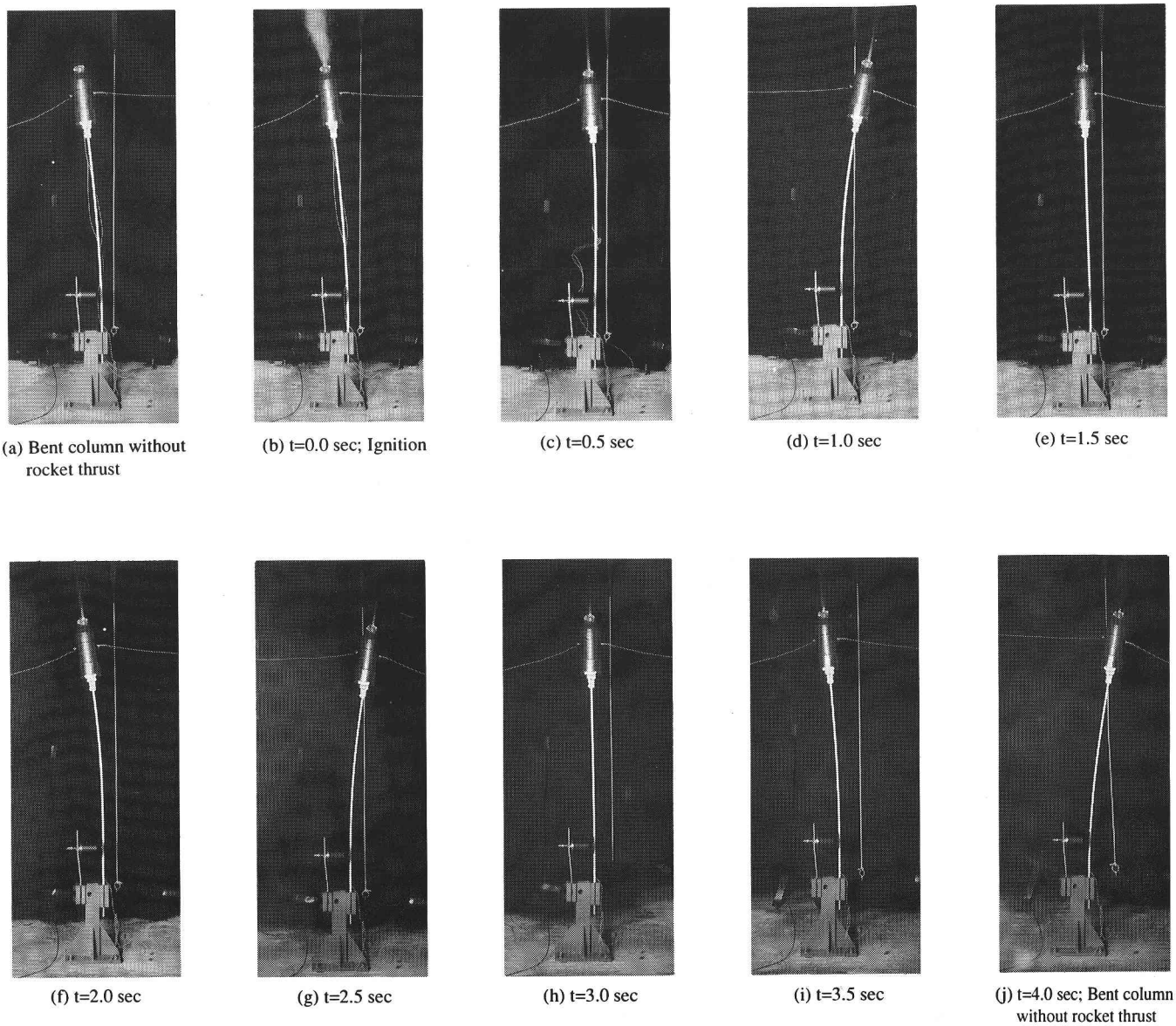

(a) Bent column without rocket thrust (b) t=0.0 sec; Ignition (c) t=0.5 sec (d) t=1.0 sec (e) t=1.5 sec

(f) t=2.0 sec (g) t=2.5 sec (h) t=3.0 sec (i) t=3.5 sec (j) t=4.0 sec; Bent column without rocket thrust

Fig. 14 Sequence of frames of the column's behavior observed in test run No. 4

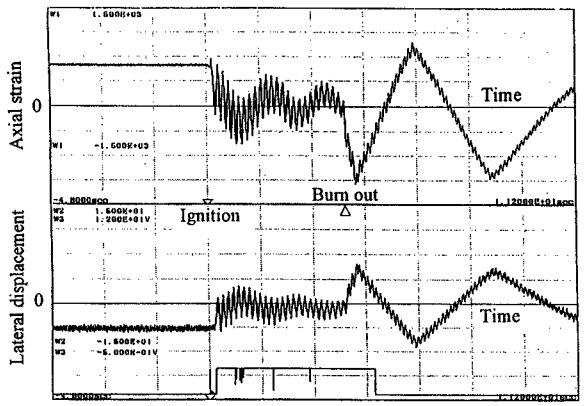

Fig. 15 Recorded axial strain and displacement for test run No. 4

8. Concluding Remarks

The present paper has reported the first experimental demonstrations of the stabilizing effect of rocket thrust on the dynamics of vertical cantilevered columns having a tip rigid body. As shown in test runs Nos. 1 and 2, rocket thrust can cause the column's oscillation with a higher frequency than when it was subjected only to a conservative load. More dramatic demonstrations were made by the test runs Nos. 3 and 4, where the bent column under a conservative load regained their straight configurations during the application of rocket thrust.

During the course of the experiment, it was found that the basic study on the dynamics of columns having a rigid body at its free end was needed, especially the effect of the mass center of the body on the dynamics and static stability of the column should be investigated both theoretically and experimentally. The authors are now working on the needed basic study to enhance the discussions of the present experimental results.

References

1. V. V. Bolotin, Nonconservative Problems of the Theory of Elastic Stability, Pergamon Press, London, (1965).
2. H. Leipholz, Stability of Elastic Systems, Sijthoff & Noordhoff, The Netherlands, (1980).
3. K. Huseyin, Vibration and Stability of Multiple Parameter Systems, Sijthoff & Noordhoff, The Netherlands, (1978).
4. T. R. Beal, Dynamic Stability of a Flexible Missile under Constant and Pulsating Thrust, AIAA Journal, Vol.3, 486, (1965)
5. G. Y. Matsumoto and C. D. Mote, Time Delay Instabilities in Large Order Systems with Controlled Follower Forces, Transactions of the ASME, Journal of Dynamic Systems, Measurement and Control, Vol.39, 330, (1972)
6. Y. P. Park and C. D. Mote, The Maximum Controlled Follower Force on a Free-Free Beam Carrying a Concentrated Mass, Journal of Sound and Vibration, Vol.98, 247, (1985)
7. D. J. McGill, Column Instability under Weight and Follower Loads, Journal of the Engineering Mechanics Division, ASCE, Vol.97, 629, (1971).
8. Y. Sugiyama and H. Kawagoe, Vibration and Stability of Elastic Columns under the Combined Action of Uniformly Distributed Vertical and Tangential Forces, Journal of Sound and Vibration, Vol.38, 341,(1975)
9. Z. Celep, On the Vibration and Stability of Beck's Column Subjected to Vertical and Follower Forces, ZAMM, Vol.57, 555, (1977).
10. B. N. Rao and G. V. Rao, Applicability of the Static or Dynamic Criterion for the Stability of a Cantilever Column under a Tip-concentrated Subtangential Follower Force, Journal of Sound and Vibration, Vol.120, No.1, 197, (1987).
11. B. N. Rao and G. V. Rao, Stability of a Cantilever Column under a Tip-Concentrated Subtangential Follower Force, with the Value of Subtangential Parameter Close to or Equal to 1/2, Journal of Sound and Vibration, Vol.125, No.1, 181, (1988).
12. Y. Sugiyama and K. A. Mladenov, Vibration and Stability of Elastic Columns Subjected to Triangularly Distributed Sub-tangential Forces, Journal of Sound and Vibration, Vol.88, No.4, 447, (1983).
13. B. J. Ryu and Y. Sugiyama, Dynamic Stability of Cantilevered Timoshenko Columns Subjected to a Rocket Thrust, Computers and Structures, Vol.51, 331, (1994).
14. Y. Sugiyama, K. Katayama and S. Kinoi, Flutter of Cantilevered Column under Rocket Thrust, Journal of Aerospace Engineering, Vol.8, No.1, 9, (1995).
15. Y. Sugiyama, J. Matsuike, B. J. Ryu, K. Katayama, S. Kinoi and N. Enomoto, Effect of Concentrated Mass on Stability of Cantilevers under Rocket Thrust, AIAA Journal, Vol.33, No.3, 499, (1995).